

Mutual-inductance route to the paramagnetic Meissner effect in two-dimensional Josephson-junction arrays

Cinzia De Leo and Giacomo Rotoli*

Dipartimento di Energetica Universita' dell'Aquila, Localita' Monteluco, Roio Poggio I67040, L'Aquila, Italy

Paola Barbara

Department of Physics, Georgetown University, Washington, DC 20057

A. P. Nielsen and C. J. Lobb

Center for Superconductivity Research, University of Maryland, College Park, Maryland 20742

(Received 8 March 2001; published 24 September 2001)

We simulate two-dimensional Josephson-junction arrays, including full mutual-inductance effects, as they are cooled below the transition temperature in a magnetic field. We show numerical simulations of the array magnetization as a function of position, as detected by a scanning superconducting quantum interference device which is placed at a fixed height above the array. The calculated magnetization images show striking agreement with the experimental images obtained by Nielsen *et al.* [Phys. Rev. B **62**, 14 380 (2000)]. The average array magnetization is found to be paramagnetic for many values of the applied field, confirming that paramagnetism can arise from magnetic screening in multiply connected superconductors without the presence of *d*-wave superconductivity.

DOI: 10.1103/PhysRevB.64.144518

PACS number(s): 74.20.-z, 74.50.+r, 75.20.-g

A dc paramagnetic susceptibility, reported first by Braunschweig *et al.*¹ for BSCCO, occurs in many high- T_c superconductors when cooled through their transition temperature in an external magnetic field. This surprising result, known as the paramagnetic Meissner effect (PME), contrasts with the standard diamagnetic response of classical superconductors and has been the subject of extensive investigations for the last ten years.

Some theoretical work² suggested that the PME provided indirect evidence for *d*-wave symmetry in the superconducting order parameter. In this picture, π junctions formed between misaligned grains were the cause of the anomalous magnetic response.

PME observed in low- T_c superconductors with *s*-wave order parameters³ demonstrated that π junctions were not required for the PME. Theories for the PME were developed, advocating nonequilibrium phenomena such as flux compression,⁴ surface barriers,⁵ and a giant vortex state.⁶ However, in the case of high- T_c samples like BSCCO, experiments¹ showed clearly that the granular nature of the samples was a crucial ingredient for the occurrence of the phenomenon. This suggested using arrays of (non- π) Josephson junctions⁷ as a model system for studying the PME in granular high- T_c samples, to test whether π junctions were also an essential ingredient. Numerical simulations of simplified Josephson junction networks (a single multijunction loop⁸ or multijunction concentric loops⁹) indeed showed a paramagnetic response. Experiments also gave indirect evidence for the PME in the ac susceptibility of arrays.¹⁰

Because of the many theories predicting the PME in both *s*- and *d*-wave superconductors, more stringent and detailed experimental tests were needed to test the relationship between paramagnetism and order parameter symmetry. Experiments using scanning superconducting quantum interference devices (SQUID's) were thus performed on high- T_c

superconductors¹¹ and on arrays of non- π junctions.¹² A scanning SQUID microscope¹³ (SSM) measures the spatial distribution of the magnetization. The complexity of the results and the experimental technique pose theoretical challenges in the qualitative and quantitative interpretation of the magnetic images.

Here we show that a model of two-dimensional (2D) arrays with full mutual-inductance interactions captures the essential facts about the PME in Josephson-junction arrays.

The arrays measured in Nielsen *et al.* had a unit cell size of $46 \mu\text{m}$ and were cooled in external flux from zero up to $12\Phi_0$ per unit cell of the array. A sketch of the array is shown in Fig. 1. The junctions had a $J_c = 600 \text{ A/cm}^2$ with a junction area of $5 \times 5 \mu\text{m}^2$ and a calculated self-inductance of $L' = 64 \text{ pH}$, yielding a $\beta_L = 2\pi L' I_0(T)/\Phi_0 = 30$ at 4.2 K. The experiment involved cooling the array in an externally applied field and then measuring the magnetization with the field still applied. These parameters are similar to those in BSCCO which exhibits the PME (Ref. 11) and are the parameters used here.

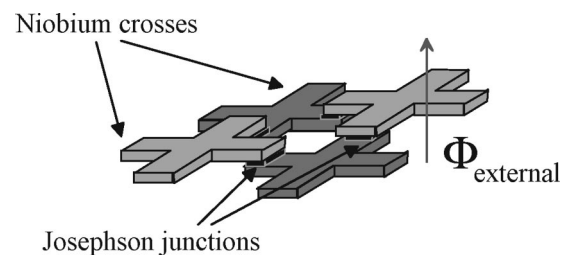


FIG. 1. Sketch of array design. Niobium crosses are in two layers, light and dark grey. The Josephson junctions are formed at the cross overlaps, as indicated, and the external flux is applied perpendicular to the array, in the \hat{z} direction. The unit cell size is $46 \mu\text{m}$.

We simulate a network of $N_r \times N_c$ junctions.^{14–17} Using a vector notation,¹⁶ the current in each junction can be modeled by the resistively and capacitively shunted junction (RCSJ) model as

$$\vec{I}^b = I_0 \sin \vec{\varphi} + \frac{\Phi_0}{2\pi} G \vec{\varphi} + \frac{\Phi_0}{2\pi} C \ddot{\varphi}. \quad (1)$$

Here $I_0 \sin \vec{\varphi}$ represents the current through the Josephson element ($\sin \vec{\varphi}$ is the vector given by applying \sin to the components of $\vec{\varphi}$), and $(\Phi_0/2\pi) \vec{\varphi}$ is the voltage drop across the quasiparticle conductance G . Finally C and I_0 are the junction capacitance and the Josephson critical current.

To satisfy the Kirchhoff's law for the currents in each node, we define loop currents \vec{I}^s connected to the junction currents by the relationship $\vec{I}^b = \hat{K} \vec{I}^s$ (for a discussion of the role of loop currents, cf. Refs. 15 and 17) where the matrix \hat{K} depends on the array geometry. The fluxoid quantization rule for each elementary loop in the array gives another set of equations:

$$\hat{M} \vec{\varphi} = 2\pi \vec{n} - 2\pi \vec{f} + \frac{2\pi L'}{\Phi_0} \hat{L} \vec{I}^s, \quad (2)$$

where \hat{M} performs the (oriented) sum of the phases around a loop; the vector \vec{f} represents the normalized flux $\phi^{ext} = f\Phi_0$ due to an external field in each loop, i.e., the so-called frustration; \vec{n} is a vector of “quantum numbers” for the flux quanta in each loop; and the last term is the field induced by the currents flowing in all other loops of the array ($\phi^{induced} = L' \hat{L} \vec{I}^s$). The matrix \hat{L} , the mutual inductance matrix of the array (normalized to the self-inductance of the single loop), represents the mutual coupling between loops in the arrays. Here we compute \hat{L} by a thin-wire approximation except for the self-inductance of a single loop (cf. Ref. 17). Inserting the fluxoid quantization in $\vec{I}^b = \hat{K} \vec{I}^s$, using Eq. (1) we obtain a system of equations in normalized units, containing only the phase variables:

$$\frac{\beta_L}{2\pi} \sin \vec{\varphi} + \sqrt{\frac{\beta_L}{\beta_C}} \vec{\varphi}_r + \vec{\varphi}_n = \hat{K} \hat{L}^{-1} \vec{m}. \quad (3)$$

Here time is normalized to a cell frequency ($\omega^{-2} = L' C$) and the usual Stewart-McCumber parameter appears, $\beta_C = 2\pi I_0(T) C / \Phi_0 G^2$. The term \vec{m} represents the normalized loop magnetization [cf. Eq. (2)]. An explicit form for magnetization can be written as follows by inverting the static form of Eq. (3):

$$\vec{m} = \frac{\beta_L}{2\pi} \hat{L} (\hat{K}^T \hat{K})^{-1} \hat{K}^T \sin \vec{\varphi}, \quad (4)$$

which generalizes the single-loop equation, Eq. (1) of Nielsen *et al.* In the case of a single loop, for large β_L , there are at least four states which are nondegenerate and that are either diamagnetic or paramagnetic. The lowest-energy states are diamagnetic for $l < f < l + 1/2$, with l integer, and paramagnetic for $l + 1/2 < f < l + 1$. For a single loop, half the

states are diamagnetic and half are paramagnetic. This contrasts with the experiments on large arrays by Nielsen *et al.* that show a clear prevalence of paramagnetism for $f \gtrsim 3$. In other words, the single-loop model cannot explain the experimental results, even qualitatively.

We can do a mean-field type of treatment of the temperature dependence by using the fact that β_C and β_L are the only temperature-dependent quantities in these equations. Thus, we simulated field cooling in the arrays solving Eq. (3) for the phases and calculating the resulting currents and magnetization. The simulation starts with a zero screening term in the equation, $\beta_L = 0$ and $\beta_C = 0$, as representing $T \gg T_c$. Nonzero frustration f was fixed in the beginning of the simulation. Then, β_L and β_C are increased in steps, until they reach their final, low-temperature value. The dynamical terms, i.e., $\ddot{\varphi}$ and $\dot{\varphi}$, go to zero after a transient. A variable transient time permits control of the speed of the simulated field cooling process. We used parameters similar to the experiments,¹² i.e., $\beta_L(T=4.2 \text{ K}) = 30$, $\beta_C(T=4.2 \text{ K}) = 66$. The transient time for each step increase in β_L ranges from 80 to 400 normalized time units, and a typical run takes 30 steps. The initial conditions for the array are chosen with all the phases being zero and a random distribution of “quantum numbers” \vec{n} , simulating the disorder due to the initial diffusion of flux quanta, when the Josephson energy barriers are small. Each component of \vec{n} was chosen using the cernlib routine RANLUX which generates uniformly distributed random numbers. Simulations of large arrays (10×40) take some time, so we have evaluated the mean magnetization for about five statistical realizations of each frustration value. For simulations on smaller arrays, which require much less computation time (e.g., 10×10), we have collected data on the mean magnetization for at least for ten statistical realizations of each frustration value. The mean magnetization of the final solution varied by no more than 2% for both array sizes. Thus we are confident that our results on the large arrays reflect the behavior of a real large array. Details of the integration routine are described in Filatrella *et al.*¹⁷

In order to have a significant comparison between the numerical simulations and the experiments, we take into account the SQUID-sample separation at a nonzero distance z above the array. Typical values of z have been chosen within the limits indicated by Ref. 12, 40–60 μm , and we normalized z to the array unit cell size, 46 μm . The field at a distance z was built by superposition of the fields generated by the currents. Each current in the array is modeled using the thin-wire approximation.¹⁸

Next, the flux within a square corresponding to the SQUID area was calculated for different positions above the array. We chose to calculate positions corresponding to the centers of the array loops (i.e., one point per loop) at distance z above them.

Figure 2 reports the field-cooled magnetization for a 10×40 array with $f = 1.2$ and clearly shows a diamagnetic behavior both locally and in the average magnetization. Figures 2(a) and 2(b), respectively, show the magnetization at $z = 0$ and $z = 1$. Figures 3 and 4 show the same array for $f = 4.8$ and $f = 12.2$: Figures 3(a) and 4(a) report the magnetization

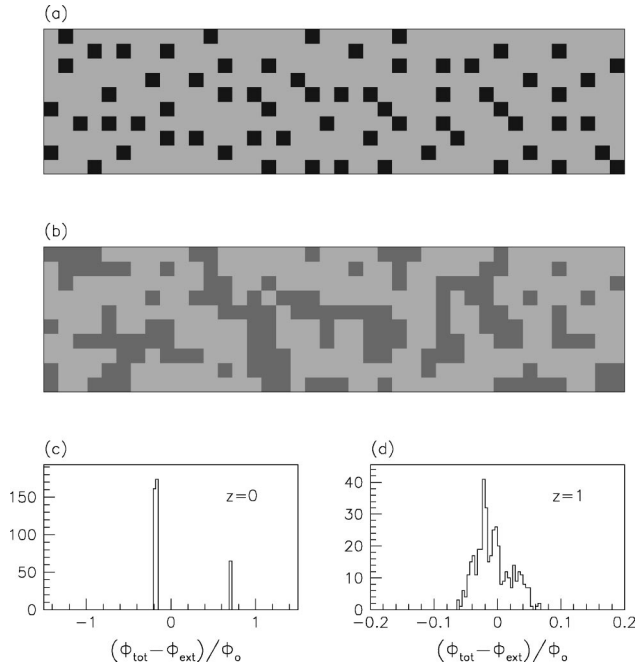


FIG. 2. Simulated field-cooled 10×40 Josephson-junction array for a frustration $f=1.2$. Parameters of simulations are $\beta_L(4.2 \text{ K})=30$, $\beta_C(4.2 \text{ K})=66$. The SQUID height z is normalized to the unit cell size. (a) Image of the array magnetization at $z=0$; (b) simulated SSM image of array magnetization at $z=1$, sampled at positions corresponding to the center of array loops. The light-gray loops are the diamagnetic ones and the dark-gray loops are paramagnetic. (c) Histogram of loop magnetization at $z=0$; (d) histogram of magnetization as read by SSM at $z=1$.

at $z=0$, Figs. 3(b) and 4(b) the magnetization at $z=1$. For values of frustration above 3, the array shows an overall paramagnetic response. It is interesting to note that in all cases, at $z=0$, there is a connection between the simulated arrays and the simple single-loop picture. If, for a given value of frustration, an isolated loop is diamagnetic (lowest-energy state), for the same value of frustration the simulated array shows a larger number of diamagnetic loops. These diamagnetic loops form a “sea” in which a few paramagnetic loops stand out [cf. Figs. 2(a) and 4(a)]. If the isolated loop is paramagnetic, the sea is formed by paramagnetic loops with few diamagnetic loops in the array [cf. Fig. 3(a)].

At $z=1$ the mixing of flux lines produces a smeared flux distribution that is very similar to the experiments (cf. Ref. 12). We note that for large frustration values [cf. Figs. 4(a) and 4(b)], due to different magnetization strengths, the far-field array image is paramagnetic, although the corresponding state for an isolated loop is diamagnetic.

In Figs. 2(c), 3(c), and 4(c), histograms of the loop magnetization are reported at $z=0$. We find two peaks representing the diamagnetic ($\Phi_{tot}-\Phi_{ext}<0$) and paramagnetic ($\Phi_{tot}-\Phi_{ext}>0$) loops. The peak position essentially corresponds to single-loop values for the same frustration. The peak width is determined by mutual inductance effects. Generally only two magnetization peaks are found, one diamagnetic and one paramagnetic (with the exception of a few loops in the $f=4.8$ case, which show a higher value of para-

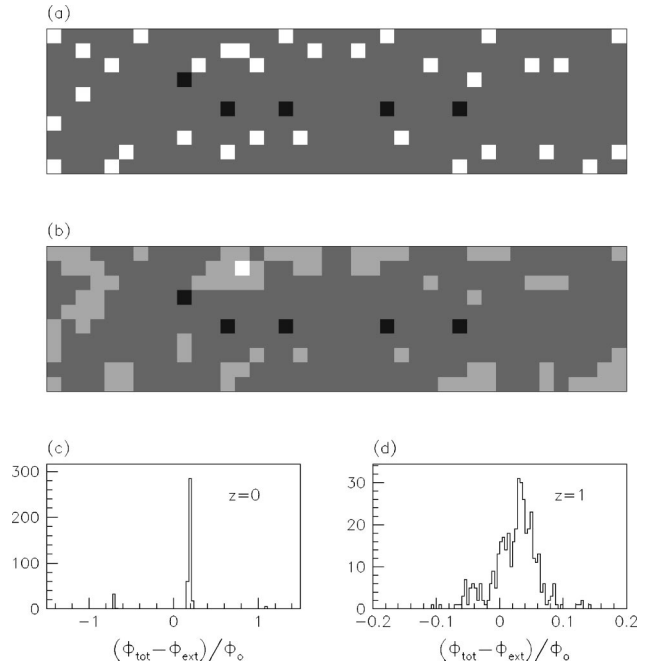


FIG. 3. The same simulated field-cooled array of Fig. 2 for $f=4.8$. (a) Image of the array magnetization at $z=0$; (b) simulated SSM image of array magnetization at $z=1$, sampled at positions corresponding to the center of array loops. The light-gray loops are the diamagnetic ones. (c) Histogram of loop magnetization at $z=0$; (d) histogram of magnetization values as read by SSM at $z=1$.

magnetic magnetization; cf. Fig. 3). The majority loops magnetize weakly whereas the minority loops magnetize strongly. Figures 2(d), 3(d), and 4(d) show the histograms evaluated at $z=1$. Similarly to the measured images, we observe a smearing effect: Histogram peaks merge, so that the overall distributions appear similar to the experimental ones. Merging of histogram peaks starts approximately at $z \approx 0.3$. The results discussed for Figs. 2, 3, and 4 can be extended to other frustration values:¹⁹ Simulations show that for $l < f < l + 1/2$, with l integer, the diamagnetic loops predominate in number, whereas for $l + 1/2 < f < l + 1$ the paramagnetic loops dominate. For $f = l + 1/2$ the solution tends to have an equal number of diamagnetic and paramagnetic loops. The magnetization strength shows a more subtle behavior: For $l < f < l + 1/2$ the strongest magnetization is paramagnetic; for $l + 1/2 < f < l + 1$ the strongest magnetization is diamagnetic. If the frustration equals a half integer, $f = l + 1/2$, the paramagnetic and diamagnetic peaks are of equal strength, so their average magnetization measures zero.

In Fig. 5 we report the mean magnetization over a 10×40 array, for different frustrations, at $z=1$. The mean magnetization depends on the blend of paramagnetic and diamagnetic strength in the loops and their number. A trend shifts the array magnetization toward paramagnetism, starting from $f \geq 3$. The mean magnetization depends weakly on noise: A test with different random distributions of quantum numbers shows that this accounts for an error of about 2%. Our estimation of z adds another source of error, but our simulations show that this error accounts for no more than

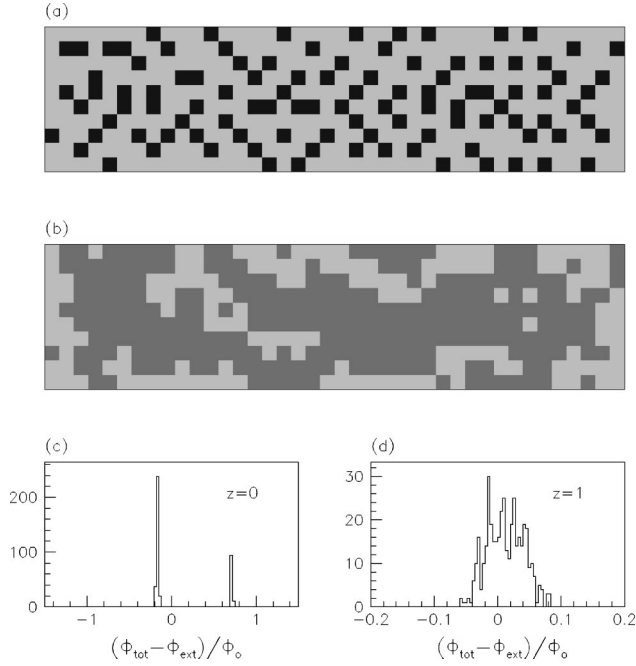


FIG. 4. The same simulated field-cooled array of Fig. 2 for $f = 12.2$. (a) Image of the array magnetization at $z=0$; (b) simulated SSM image of array magnetization at $z=1$, sampled at positions corresponding to the center of array loops. The light-gray meshes are the diamagnetic ones. (c) Histogram of loop magnetization at $z=0$; (d) histogram of magnetization values as read by SSM at $z=1$.

5%, with a z variance of 20%. On the other hand, the mean magnetization depends on the dimension of the array. A direct quantitative comparison with the experiments shows a calculated value of magnetization typically lower. Magnetization strongly depends on the array dimension, so the results presented in Fig. 5 can be only qualitatively compared with experiments, in which arrays are larger. We report only positive frustration ($f > 0$) because Eq. (3) is symmetric, changing the sign of frustration (the same array viewed from below simply maintains the same paramagnetic and diamagnetic loops).

We note that in all cases, i.e., both diamagnetic and paramagnetic, diamagnetic behavior prevails near the array edges. This agrees with the experiments, which show a similar behavior. According to Ref. 12 this occurs because the array screens the field by generating diamagnetic currents on the array boundary and, as a consequence, induces paramagnetic currents in the interior of the array, thus generating an overall paramagnetic offset.

To further support this view, we calculated the densities of paramagnetic loops at the boundary and in the bulk of the array. We find that there is a clear divergence between two

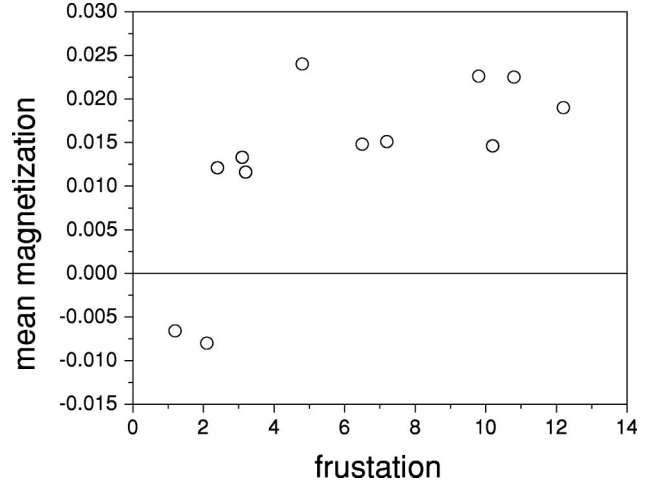


FIG. 5. Dependence of mean array magnetization on frustration for a 10×40 array. Parameters of simulations are $\beta_L(4.2 \text{ K}) = 30$, $\beta_C(4.2 \text{ K}) = 66$, and $z = 1$.

data sets with an increase of bulk density ρ_k with respect to boundary density ρ_b for frustration $f \gtrsim 3$. For example, at $f = 1.2$ the two densities are roughly equal, $\rho_b = N_{para}/N_{boundary} \approx 0.156$ and $\rho_k = N_{para}/N_{total} \approx 0.162$, but at $f = 12.2$ at the boundary we have $\rho_b \approx 0.11$ and in the bulk $\rho_k \approx 0.26$. Tests on smaller arrays show that paramagnetic behavior for $m < f < m + 1/2$ arises about for $N \sim 5$; this is roughly the value predicted from Eq. (4) of Ref. 12 for $\beta_L = 30$.

In conclusion, the PME in Josephson-junction arrays can be reproduced via numerical simulations which include the full inductance matrix. The simulation results compare favorably to experimental results: Paramagnetism dominates field cooling for large arrays. Simulations also show that the single-loop model is the basic building block describing the field-cooled array behavior. Mutual-inductance interactions create the actual distribution of loop magnetization in the arrays. The resulting mean magnetization is the product of both single-loop states and their occupancy. The observed dominant paramagnetism, in both experiments and simulations, arises from an energetic preference for paramagnetic loops interior to the array.

Beyond this study, a number of open problems still remain to be analyzed. Among these are simulations of larger arrays in order to make more detailed comparisons with experiments and the study of the effect of cooling time and transient dynamics of the array.

We acknowledge support by MURST COFIN98 project “Dynamics and Thermodynamics of vortex structures in superconductive tunneling,” by AFOSR under Grant No. F4620-98-1-0072, and by the NSF under Grant No. DMR 9732800.

*Also at Unita’ INFM, Universita’ dell’Aquila, Localita’ Monteluco, Roio Poggio I67040, L’Aquila, Italy.

¹W. Braunisch *et al.*, Phys. Rev. Lett. **68**, 1908 (1992).

²M. Sigrist and T.M. Rice, J. Phys. Soc. Jpn. **61**, 4283 (1992).

³D.J. Thompson, M.S.M. Minhaj, L.E. Wenger, and J.T. Chen, Phys. Rev. Lett. **75**, 529 (1995); P. Kostic *et al.*, Phys. Rev. B **53**, 791 (1996).

⁴A.E. Koshelev and A.I. Larkin, Phys. Rev. B **52**, 13 559 (1995).

- ⁵V.V. Moschalkov, X.G. Qiu, and V. Bruyndoncx, *Phys. Rev. B* **55**, 11 793 (1997); P.S. Deo, V.A. Schweigert, F.M. Peeters, and A.K. Geim, *Phys. Rev. Lett.* **79**, 4653 (1997).
- ⁶P.S. Deo, V.A. Schweigert, and F.M. Peeters, *Phys. Rev. B* **59**, 6039 (1999).
- ⁷R.S. Newrock, C.J. Lobb, U. Geigenmüller, and M. Octavio, *Solid State Phys.* **54**, 263 (2000).
- ⁸C. Auletta, P. Caputo, G. Costabile, R. De Luca, S. Pace, and A. Saggese, *Physica C* **235-240**, 3314 (1994).
- ⁹C. Auletta, G. Raiconi, R. De Luca, and S. Pace, *Phys. Rev. B* **51**, 12 844 (1995).
- ¹⁰F.M. Araujo-Moreira, P. Barbara, A.B. Cawthorne, and C.J. Lobb, *Phys. Rev. Lett.* **78**, 4625 (1997); P. Barbara, F.M. Araujo-Moreira, A.B. Cawthorne, and C.J. Lobb, *Phys. Rev. B* **60**, 7489 (1999).
- ¹¹J.R. Kirtley, A.C. Mota, M. Sgrist, and T.M. Rice, *J. Phys.: Condens. Matter* **10**, L97 (1998).
- ¹²A.P. Nielsen, A.B. Cawthorne, P. Barbara, F.C. Wellstood, C.J. Lobb, R.S. Newrock, and M.G. Forrester, *Phys. Rev. B* **62**, 14 380 (2000).
- ¹³R.C. Black, A. Mathai, F.C. Wellstood, E. Dantsker, A.H. Miklich, D.T. Nemeth, J.J. Kingston, and J. Clarke, *Appl. Phys. Lett.* **62**, 2128 (1993).
- ¹⁴J.R. Phillips, H.S.J. van der Zant, J. White, and T.P. Orlando, *Phys. Rev. B* **47**, 5219 (1993).
- ¹⁵D. Dominguez and J. José, *Phys. Rev. B* **53**, 11 692 (1996).
- ¹⁶C. Lucheroni, *Phys. Rev. B* **55**, 6559 (1997).
- ¹⁷G. Filatrella, A. Petraglia, and G. Rotoli, *Eur. Phys. J. B* **12**, 23 (1999).
- ¹⁸C. De Leo and G. Rotoli, presented at the 8th International Superconductive Electronics Conference, ISEC'01, Osaka, 19–22 June 2001 (unpublished).
- ¹⁹C. De Leo and G. Rotoli (unpublished). See material at www.ing.univaq.it/energetica/research/Fisica/supgru.htm